

Finite-time complex projective synchronization of fractional-order complex-valued uncertain multi-link network and its image encryption application

Yong-Bing Hu(胡永兵), Xiao-Min Yang(杨晓敏), Da-Wei Ding(丁大为), and Zong-Li Yang(杨宗立)
Citation: Chin. Phys. B, 2022, 31 (**11**): 110501. DOI: 10.1088/1674-1056/ac7869

What follows is a list of articles you may be interested in

The dynamics of a memristor-based Rulkov neuron with fractional-order difference

Yan-Mei Lu(卢艳梅), Chun-Hua Wang(王春华), Quan-Li Deng(邓全利), and Cong Xu(徐聪)
Chin. Phys. B, 2022, 31 (**6**): 060502. DOI: 10.1088/1674-1056/ac539a

Controlling chaos and supressing chimeras in a fractional-order discrete phase-locked loop using impulse control

Karthikeyan Rajagopal, Anitha Karthikeyan, and Balamurali Ramakrishnan
Chin. Phys. B, 2021, 30 (**12**): 120512. DOI: 10.1088/1674-1056/ac1b83

Analysis and implementation of new fractional-order multi-scroll hidden attractors

Li Cui(崔力), Wen-Hui Luo(雒文辉), and Qing-Li Ou(欧青立)
Chin. Phys. B, 2021, 30 (**2**): 020501. DOI: 10.1088/1674-1056/abbbe4

Chaotic analysis of Atangana-Baleanu derivative fractional order Willis aneurysm system

Fei Gao(高飞), Wen-Qin Li(李文琴), Heng-Qing Tong(童恒庆), Xi-Ling Li(李喜玲)
Chin. Phys. B, 2019, 28 (**9**): 090501. DOI: 10.1088/1674-1056/ab38a4

Turing pattern in the fractional Gierer-Meinhardt model

Yu Wang(王语), Rongpei Zhang(张荣培), Zhen Wang(王震), Zijian Han(韩子健)
Chin. Phys. B, 2019, 28 (**5**): 050503. DOI: 10.1088/1674-1056/28/5/050503

Finite-time complex projective synchronization of fractional-order complex-valued uncertain multi-link network and its image encryption application

Yong-Bing Hu(胡永兵)[1], Xiao-Min Yang(杨晓敏)[1], Da-Wei Ding(丁大为)[1,2,†], and Zong-Li Yang(杨宗立)[1]

[1] *School of Electronics and Information Engineering, Anhui University, Hefei* 230601, *China*
[2] *National Engineering Research Center for Agro-Ecological Big Data Analysis & Application, Anhui University, Hefei* 230601, *China*

(Received 4 May 2022; revised manuscript received 7 June 2022; accepted manuscript online 14 June 2022)

Multi-link networks are universal in the real world such as relationship networks, transportation networks, and communication networks. It is significant to investigate the synchronization of the network with multi-link. In this paper, considering the complex network with uncertain parameters, new adaptive controller and update laws are proposed to ensure that complex-valued multilink network realizes finite-time complex projective synchronization (FTCPS). In addition, based on fractional-order Lyapunov functional method and finite-time stability theory, the criteria of FTCPS are derived and synchronization time is given which is associated with fractional order and control parameters. Meanwhile, numerical example is given to verify the validity of proposed finite-time complex projection strategy and analyze the relationship between synchronization time and fractional order and control parameters. Finally, the network is applied to image encryption, and the security analysis is carried out to verify the correctness of this method.

Keywords: multi-links network, fractional order, complex-valued network, finite-time complex projective synchronization, image encryption

PACS: 05.45.Gg, 05.45.Xt **DOI:** 10.1088/1674-1056/ac7869

1. Introduction

Complex networks (CNs) are effective system modeling tools in the real world, every network can be described in terms of nodes and edges, where each edge represents a connection between nodes. Multi-link networks[1–3] are the networks that have more than one connection between two nodes. There are numerous multilink networks in life, such as relationship networks, transportation networks, and communication networks.[4,5] For example, in the transportation networks, the speeds of transmission among highway network, railway network, and airline network are different from each other, which can be seen as that the connections of transportation network have different delays. In Refs. [6,7], the complex multi-link network is split into sub-networks with delay so as to describe the delay characteristics of multi-links network. As a special case of multi-link network, single-link network has been investigated by many researchers. Nevertheless, little attention has been paid to multi-link networks. Therefore, complex dynamic networks with multiple links have certain research value.[8,9]

Synchronization is an important research topic in CNs. Researchers have studied many synchronization methods, such as projective synchronization,[10] pinning synchronization,[11] and exponential synchronization.[12,13] Projective synchronization (PS) reflects the proportional relationship between synchronization states by introducing a scaling factor. In Ref. [14], Sha *et al*. used the control method based on uncertainty and disturbance estimation and linear feedback to accomplish PS in complex chaotic systems. As an extension of PS, complex projective synchronization (CPS) leads to synchronization complexity and diversity because its scale factor is a complex number. In Ref. [15], using the stability theorem of the fractional-order systems with multiple delays, Ding *et al*. achieved CPS in memristive neural network. The CPS occurs asymptotically and it has unbounded convergence time. In fact, the synchronization is often required to accomplish in a finite time. The finite-time control technology is made realize finite-time synchronization in CNs.[16,17] By using a functional scaling factor, Wang *et al*. investigated finite-time function projective synchronization for multi-link networks with time-varying delay.[18] In Ref. [19], Zhao *et al*. realized the fixed-time synchronization and finite-time synchronization in CNs with multilink by using Lyapunov function and linear matrix inequality. In Ref. [20], Zheng *et al*. studied the decay synchronization of complex multi-link time-varying dynamic network.

In the existing literature concerning multi-link networks, most of researches are based on integer-order multi-link networks. As a mathematical element that deals with integrals and derivatives in the form of non-integer order, fractional calculus not only has more degrees of freedom than integer calculus, but also possesses unique properties including heredity and infinite memory. At present, fractional calculus has been

†Corresponding author. E-mail: dwding@ahu.edu.cn

© 2022 Chinese Physical Society and IOP Publishing Ltd

widely used in CNs which is called fractional order CNs. For example, in Ref. [21], Li *et al*. used hybrid impulsive control to investigate the global synchronization for two fractional order CNs with non-delayed and delayed coupling. Bao *et al*. achieved the synchronization of fractional order neural networks with output coupling on the basis of fractional-order Lyapunov function and linear matrix inequalities.[22] Nevertheless, as far as we know, the research results of fractional order multi-link networks are few until now. Therefore, it is significant to incorporate fractional calculus into multi-links networks.

Comparing with real-valued networks, the applications of complex-valued networks are more extensive. For example, there are more variables and transmitted information in complex-valued networks, and the security of transmitted information is also greatly enhanced. Furthermore, complex-valued networks show complex dynamic behaviors and can describe some physical phenomena such as electromagnetic field amplitude, and rotating fluid.[23,24] Yang *et al*. studied the quasi-projective synchronization of fractional order complex-valued neural networks via linear control strategy.[25] In Ref. [26], Xu *et al*. used complex function theory and combined Lyapunov method with graph theory to address finite-time synchronization for fractional order complex-valued multi-weighted dynamical networks.

Because the fluctuation of system parameters and the disturbance of external environment are always inevitable, they lead to the uncertainty of system parameters. When analyzing system dynamic characteristics, parameter uncertainties should be considered because they may have influence on the synchronization performance and system stability. Therefore, uncertain complex networks are valuable.[27–30] In Ref. [31], making use of the properties of fractional calculus, Li *et al*. accomplished finite-time synchronization for fractional order complex dynamical networks (FOCDNs) with unknown parameters and the parameters were identified. Du *et al*. investigated synchronization of all nodes in FOCDNs with uncertain parameters by adaptive control strategy.[32] Yang *et al*. designed two different controllers to study finite-time lag synchronization of uncertain complex networks with impulsive disturbance.[33]

In addition, synchronization can improve the security of image transmission and has great applications in secure communication. Considering the highly nonlinear nature of complex networks and non-locality of fractional order chaotic systems, fractional order complex networks are worth applying to image encryption.[34] Wang and Yang proposed a new encryption system algorithm for encrypting/decrypting color images.[35] The DNA encoding algorithm has advantages of high parallelism, high storage capacity and low power consumption in the field of image encryption.[36,37] Moreover, image encryption based on complex network and DNA approach has a good encryption effect.

From the above analysis, this paper is to address FTCPS of fractional order complex-valued multi-links network and applies it to the image encryption. The main difficulty is how to deal with the delay problem in fractional order multi-link networks. The synchronization is realized via adaptive controller. The criteria of FTCPS are obtained by using fractional-order Lyapunov functional method and finite-time stability theory. Two examples are used to verify the validity of theoretical results. The main contributions are listed below. First, most of researches are based on integer-order multi-links networks, but we extend the integer-order multi-link networks to the fractional-order networks to make the results more general. Secondly, most of previous multi-link networks are real-valued, but this paper focuses on complex-valued field. Then, considering the uncertainty of network parameters, new update laws are designed and the control strategy of FTCPS is proposed. Compared with the infinite-time synchronization, this finite-time synchronization can improve convergence performance. Finally, the criteria of FTCPS are derived and the relationship between synchronization time and fractional order and control parameters is analyzed. Besides, the network is applied to image encryption and the security analysis is carried out.

The rest of this paper is structured as follows. In Section 2 some preliminaries and network description are introduced. In Section 3, the main results are demonstrated. Numerical example and image encryption application are provided in Section 4 to verify the validity of the proposed results. In Section 5 some conclusions are drawn from the researches of this paper.

Notations: In this paper, for any $x\in C^n$, x^{r}, x^{i}, and x^{H} represent the real parts, imaginary parts, and conjugate transpose of x, respectively. $\|x\| = \sqrt{x^{\mathrm{H}}x}$ represents the norm of x. For Hermite matrix Q, if $Q>0$, then Q is positive-definite; on the contrary, Q is negative definite. $\lambda_{\max}(\cdot)$ and $\lambda_{\min}(\cdot)$ manifest the maximum eigenvalue and the minimum eigenvalue of corresponding matrix. $\otimes$ denotes Kronecker product.

2. Preliminaries and network description

We introduce some definitions and lemmas in this section, which are helpful for our later research.

Definition 1[38] Caputo derivative of order α for a function $f(t)\in C^n([t_0,+\infty)R)$ (the set of all n-order continuous differentiable functions on $[t_0,+\infty)$) is defined as

$$ {}_{t_0}^{C}D_t^{\alpha} f(t) = \frac{1}{\Gamma(n-\alpha)} \int_{t_0}^{t} \frac{f^{(n)}(\tau)}{(t-\tau)^{\alpha+1-n}} \mathrm{d}\tau, $$

where $t\geq t_0$, n is a positive integer, $n-1<\alpha<n$. $\Gamma(\cdot)$ is the

Gamma function. Particularly, when $0<\alpha<1$,

$$ {}_{t_0}^{C}D_t^{\alpha} f(t)=\frac{1}{\Gamma(1-\alpha)}\int_{t_0}^{t}\frac{f'(\tau)}{(t-\tau)^{\alpha}}\,\mathrm{d}\tau. $$

In this paper, we consider the fractional order complex-valued multi-links network with uncertain parameters, which is described by

$$ \begin{aligned} {}_{t_0}^{C}D_t^{\alpha} x_i(t) &= f(x_i(t))+g(x_i(t))\beta_i \\ &\quad+\sum_{l=0}^{m-1}\sum_{j=1}^{N} a_{ij}^{l}\boldsymbol{\Gamma}x_j(t-\tau_l), \quad i=1,2,\ldots,N, \end{aligned} \tag{1} $$

where α denotes the fractional order and satisfies $0<\alpha<1$, $x_i(t)=(x_{i1}(t),x_{i2}(t),\ldots,x_{in}(t))^{\mathrm{T}}\in C^n$ refers to the complex variable state vector of the i-th node, $f(x_i(t))$ is an $n\times 1$ complex vector function, $g(x_i(t))$ is an $n\times n$ complex matrix function, $\beta_i=(\beta_{i1},\beta_{i2},\ldots,\beta_{in})^{\mathrm{T}}$ is the unknown parameter vector, $\boldsymbol{\Gamma}=\mathrm{diag}(\gamma_1,\gamma_2,\ldots,\gamma_n)>0$ is the inner coupling matrix, τ_l $(l=0,1,\ldots,m-1)$ is the coupling delay of sub-network and $\tau_0=0$, and $(a_{ij}^0)_{N\times N}$ and $(a_{ij}^l)_{N\times N}$ $(l=1,\ldots,m-1)$ represent the zero sub-network's and the l-th sub-network's topological structure on basis of delays. If there is a connection between nodes i and j, then $a_{ij}^l=a_{ji}^l>0$, or else $a_{ij}^l=a_{ji}^l=0$. And define $a_{ii}^l=-\sum\limits_{j=1,j\neq i}^{N}a_{ij}^l$.

Considering $s(t)$ as a reference node which satisfies the following dynamic equation:

$$ {}_{t_0}^{C}D_t^{\alpha} s(t)=f(s(t))+g(s(t))\vartheta, \tag{2} $$

where $\vartheta=(\vartheta_1,\vartheta_2,\ldots,\vartheta_n)^{\mathrm{T}}$ is the unknown system vector.

Definition 2[39] The fractional order complex-valued uncertain networks (1) and (2) are said to realize CPS if they satisfy

$$ \|x_i(t)-vs(t)\|=0, \quad i=1,2,\ldots,N, $$

where projection factor $v=a+b\mathrm{j}$ is an arbitrary complex number, a and b represent its real part and imaginary part, respectively, and $\mathrm{j}=\sqrt{-1}$ denotes imaginary unit.

Remark 1 When $v=1$, the complete synchronization is achieved. When $v=-1$, the anti-synchronization is realized. When $v=a$ the projection synchronization is realized.

Lemma 1[40] Let $x(t)\in C^n$ be a complex-valued vector which is differentiable. M is a constant positive-definite Hermitian matrix. Then, for all $t\geq t_0$ and $0<\alpha<1$, the following inequality holds:

$$ \begin{aligned} &{}_{t_0}^{C}D_t^{\alpha}\left(x^{\mathrm{H}}(t)Mx(t)\right) \\ &\leq x^{\mathrm{H}}(t)M\left({}_{t_0}^{C}D_t^{\alpha}x(t)\right)+\left({}_{t_0}^{C}D_t^{\alpha}x^{\mathrm{H}}(t)\right)Mx(t). \end{aligned} $$

Lemma 2[41] For any $X,Y\in C^n$ and constant $\mu>0$, if P is a positive-definite Hermitian matrix, then

$$ X^{\mathrm{H}}PY+Y^{\mathrm{H}}PX\leq\mu X^{\mathrm{H}}PX+\frac{1}{\mu}Y^{\mathrm{H}}PY. $$

Lemma 3[42] For $\delta_r\geq 0$ with $r=1,2,\ldots,k$, $0\leq\sigma\leq 1$, then

$$ \sum_{r=1}^{k}\delta_r^{\sigma}\geq\left(\sum_{r=1}^{k}\delta_r\right)^{\sigma}. $$

Lemma 4[43] Assume that a continuous, positive-define function $V(t)$ satisfies the following fractional-order differential inequality:

$$ {}_{t_0}^{C}D_t^{\alpha}V(t)\leq -cV^{\eta}(t), $$

where $c>0$, $0<\eta<\alpha$ and they are all constants. Then $V(t)$ satisfies the following inequality:

$$ V^{\alpha-\eta}(t)\leq V^{\alpha-\eta}(t_0)-\frac{c\Gamma(1+\alpha-\eta)(t-t_0)^{\alpha}}{\Gamma(1+\alpha)\Gamma(1-\eta)}, \quad t_0\leq t\leq t_1 $$

and $V(t)=0$ for all $t\geq t_1$, here t_1 is given by

$$ t_1=t_0+\left(\frac{\Gamma(1+\alpha)\Gamma(1-\eta)V^{\alpha-\eta}(t_0)}{c\Gamma(1+\alpha-\eta)}\right)^{1/\alpha}. $$

Remark 2 Compared with the finite-time synchronization issue of integer-order systems, Lemma 4 has a wide range of applications, and the Lemma 4 can be used to study the finite-time stability or synchronization issue for fractional-order systems or FOCDNs.

3. Main results

In this section, we put forward an adaptive controller for accomplishing FTCPS in the fractional-order complex-valued uncertain multi-links network.

Network (1) can be rewritten as follows:

$$ \begin{aligned} {}_{t_0}^{C}D_t^{\alpha} x_i(t) &= f(x_i(t))+g(x_i(t))\beta_i \\ &\quad+\sum_{l=0}^{m-1}\sum_{j=1}^{N} a_{ij}^{l}\boldsymbol{\Gamma}x_j(t-\tau_l)+u_i(t), \\ &\quad i=1,2,\ldots,N. \end{aligned} \tag{3} $$

Defining the synchronization errors as

$$ e_i(t)=x_i(t)-vs(t), \quad i=1,2,\ldots,N, \tag{4} $$

we derive the following error system:

$$ \begin{aligned} {}_{t_0}^{C}D_t^{\alpha} e_i(t) &= f(x_i(t))+g(x_i(t))\beta_i+\sum_{l=0}^{m-1}\sum_{j=1}^{N} a_{ij}^{l}\boldsymbol{\Gamma}e_j(t-\tau_l) \\ &\quad -v(f(s(t))+g(s(t))\vartheta)+u_i(t). \end{aligned} \tag{5} $$

The controller $u_i(t)$ is designed as

$$ \begin{aligned} u_i(t) &= -f(x_i(t))-g(x_i(t))\hat{\beta}_i(t) \\ &\quad+v\left(f(s(t))+g(s(t))\hat{\vartheta}(t)\right)-r_1e_i(t) \\ &\quad-\frac{\lambda e_i(t)}{[e_i^{\mathrm{H}}(t)e_i(t)]^{\rho}}+r_2\sum_{l=1}^{m-1}e_i(t-\tau_l), \end{aligned} \tag{6} $$

where r_1 and r_2 are designed later, $\rho \in (1-\alpha, 1)$, λ is a tunable positive constant, $\hat{\beta}_i(t)$ and $\hat{\vartheta}(t)$ are the estimation of the unknown parameter vector β_i and ϑ, respectively. The parameter update laws are designed below:

$$
\begin{aligned}
{}_{t_0}^{C}D_t^{\alpha}\hat{\vartheta}(t) = &-g^{\mathrm{H}}(s(t))\,v^{\mathrm{H}}e_i(t) \\
&-\frac{\lambda\left(\hat{\vartheta}(t)-\vartheta\right)}{\left[(\hat{\vartheta}(t)-\vartheta)^{\mathrm{H}}(\hat{\vartheta}(t)-\vartheta)\right]^{\rho}},
\end{aligned} \tag{7}
$$

$$
{}_{t_0}^{C}D_t^{\alpha}\hat{\beta}_i(t) = g^{\mathrm{H}}(x_i(t))\,e_i(t) - \frac{\lambda\left(\hat{\beta}_i(t)-\beta_i\right)}{\left[(\hat{\beta}_i(t)-\beta_i)^{\mathrm{H}}(\hat{\beta}_i(t)-\beta_i)\right]^{\rho}}. \tag{8}
$$

Theorem 1 If $P_l = P_l^{\mathrm{H}}$ and constants r_1 and r_2 exist and satisfy the following inequalities:

$$
r_2(m-1)+1+\sum_{l=1}^{m-1}\lambda_{\max}\left(P_l^{\mathrm{H}}P_l\right)-2r_1<0, \tag{9}
$$

$$
r_2+1<0. \tag{10}
$$

Then, under the controller (6), networks (2) and (3) achieve CPS in a finite time

$$
t_1 = t_0+\left(\frac{\Gamma(1+\alpha)\Gamma(\rho)V^{\alpha+\rho-1}(t_0)}{2\lambda\Gamma(\alpha+\rho)}\right)^{1/\alpha}, \tag{11}
$$

where

$$
\begin{aligned}
V(t_0) = &\sum_{i=1}^{N}e_i^{\mathrm{H}}(t_0)\,e_i(t_0)+\sum_{i=1}^{N}\left(\hat{\vartheta}(t_0)-\theta\right)^{\mathrm{H}}\left(\hat{\vartheta}(t_0)-\theta\right) \\
&+\sum_{i=1}^{N}\left(\hat{\beta}_i(t_0)-\beta_i\right)^{\mathrm{H}}\left(\hat{\beta}_i(t_0)-\beta_i\right).
\end{aligned}
$$

Proof Construct Lyapunov function as follows:

$$
\begin{aligned}
V(t) = &\sum_{i=1}^{N}e_i^{\mathrm{H}}(t)\,e_i(t)+\sum_{i=1}^{N}(\hat{\vartheta}(t)-\vartheta)^{\mathrm{H}}(\hat{\vartheta}(t)-\vartheta) \\
&+\sum_{i=1}^{N}(\hat{\beta}_i(t)-\beta_i)^{\mathrm{H}}(\hat{\beta}_i(t)-\beta_i),
\end{aligned} \tag{12}
$$

and calculate the derivative of $V(t)$ based on Lemma 1, then the following inequality will be obtained:

$$
\begin{aligned}
&{}_{t_0}^{C}D_t^{\alpha}V(t) \\
\le &\sum_{i=1}^{N}[{}_{t_0}^{C}D_t^{\alpha}e_i^{\mathrm{H}}(t)\,e_i(t)+e_i^{\mathrm{H}}(t)\,{}_{t_0}^{C}D_t^{\alpha}e_i(t)] \\
&+\sum_{i=1}^{N}[{}_{t_0}^{C}D_t^{\alpha}\hat{\vartheta}^{\mathrm{H}}(t)(\hat{\vartheta}(t)-\vartheta)+(\hat{\vartheta}(t)-\vartheta)^{\mathrm{H}}\,{}_{t_0}^{C}D_t^{\alpha}\hat{\vartheta}(t)] \\
&+\sum_{i=1}^{N}[{}_{t_0}^{C}D_t^{\alpha}\hat{\beta}_i^{\mathrm{H}}(t)(\hat{\beta}_i(t)-\beta_i)+(\hat{\beta}_i(t)-\beta_i)^{\mathrm{H}}\,{}_{t_0}^{C}D_t^{\alpha}\hat{\beta}_i(t)] \\
= &\sum_{i=1}^{N}[g(x_i(t))(\beta_i-\hat{\beta}_i(t))-vg(s(t)(\vartheta-\hat{\vartheta}(t)) \\
&-r_1e_i(t)-\frac{\lambda e_i(t)}{[e_i^{\mathrm{H}}(t)e_i(t)]^{\rho}} \\
&+r_2\sum_{l=1}^{m-1}e_i(t-\tau_l)+\sum_{l=0}^{m-1}\sum_{j=1}^{N}a_{ij}^{l}\boldsymbol{\Gamma}e_j(t-\tau_l)]^{\mathrm{H}}e_i(t) \\
&+\sum_{i=1}^{N}e_i^{\mathrm{H}}(t)\left[g(x_i(t))(\beta_i-\hat{\beta}_i(t))-vg(s(t)(\vartheta-\hat{\vartheta}(t))\right. \\
&-r_1e_i(t)-\frac{\lambda e_i(t)}{[e_i^{\mathrm{H}}(t)e_i(t)]^{\rho}} \\
&\left.+r_2\sum_{l=1}^{m-1}e_i(t-\tau_l)+\sum_{l=0}^{m-1}\sum_{j=1}^{N}a_{ij}^{l}\boldsymbol{\Gamma}e_j(t-\tau_l)\right] \\
&+\sum_{i=1}^{N}\left[-g^{\mathrm{H}}(s(t))\,v^{\mathrm{H}}e_i(t)\right. \\
&\left.-\frac{\lambda(\hat{\vartheta}(t)-\vartheta)}{[(\hat{\vartheta}(t)-\vartheta)^{\mathrm{H}}(\hat{\vartheta}(t)-\vartheta)]^{\rho}}\right]^{\mathrm{H}}(\hat{\vartheta}(t)-\vartheta) \\
&+\sum_{i=1}^{N}(\hat{\vartheta}(t)-\vartheta)^{\mathrm{H}}\left[-g^{\mathrm{H}}(s(t))\,v^{\mathrm{H}}e_i(t)\right. \\
&\left.-\frac{\lambda(\hat{\vartheta}(t)-\vartheta)}{[(\hat{\vartheta}(t)-\vartheta)^{\mathrm{H}}(\hat{\vartheta}(t)-\vartheta)]^{\rho}}\right]+\sum_{i=1}^{N}\left[g^{\mathrm{H}}(x_i(t))\,e_i(t)\right. \\
&\left.-\frac{\lambda(\hat{\beta}_i(t)-\beta_i)}{[(\hat{\beta}_i(t)-\beta_i)^{\mathrm{H}}(\hat{\beta}_i(t)-\beta_i)]^{\rho}}\right]^{\mathrm{H}}(\hat{\beta}_i(t)-\beta_i) \\
&+\sum_{i=1}^{N}(\hat{\beta}_i(t)-\beta_i)^{\mathrm{H}}\left[g^{\mathrm{H}}(x_i(t))\,e_i(t)\right. \\
&\left.-\frac{\lambda\left(\hat{\beta}_i(t)-\beta_i\right)}{[(\hat{\beta}_i(t)-\beta_i)^{\mathrm{H}}(\hat{\beta}_i(t)-\beta_i)]^{\rho}}\right].
\end{aligned}
$$

Let

$$
\begin{aligned}
&e(t) = [e_1(t), e_2(t), \ldots e_N(t)]^{\mathrm{T}}, \\
&A_l = (a_{ij}^{l})_{N\times N}, \quad l = 0,1,\ldots m-1, \\
&P_l = A_l\otimes\boldsymbol{\Gamma},
\end{aligned}
$$

then it will follow that

$$
\begin{aligned}
{}_{t_0}^{C}D_t^{\alpha}V(t) \le\ & r_2\sum_{l=1}^{m-1}e^{\mathrm{H}}(t-\tau_l)e(t)+\sum_{l=1}^{m-1}e^{\mathrm{H}}(t-\tau_l)P_le(t)+e^{\mathrm{H}}(t-\tau_l)P_0e(t) \\
&+r_2\sum_{l=1}^{m-1}e^{\mathrm{H}}(t)e(t-\tau_l)+\sum_{l=1}^{m-1}e^{\mathrm{H}}(t)P_le(t-\tau_l)+e^{\mathrm{H}}(t)P_0e(t-\tau_l)-2\sum_{i=1}^{N}r_1e_i^{\mathrm{H}}(t)e_i(t) \\
&-2\lambda_i\left[\sum_{i=1}^{N}(e_i^{\mathrm{H}}(t)e_i(t))^{1-\rho}+\sum_{i=1}^{N}((\hat{\vartheta}(t)-\vartheta)^{\mathrm{H}}(\hat{\vartheta}(t)-\vartheta))^{1-\rho}+\sum_{i=1}^{N}((\hat{\beta}_i(t)-\beta_i)^{\mathrm{H}}(\hat{\beta}_i(t)-\beta_i))^{1-\rho}\right].
\end{aligned} \tag{13}
$$

According to Lemma 2, we obtain

$$\sum_{l=1}^{m-1} e^{\mathrm{H}}(t-\tau_l)e(t)+\sum_{l=1}^{m-1} e^{\mathrm{H}}(t)e(t-\tau_l)\le\sum_{l=1}^{m-1} e^{\mathrm{H}}(t-\tau_l)e(t-\tau_l)+\sum_{l=1}^{m-1} e^{\mathrm{H}}(t)e(t),$$
$$\sum_{l=1}^{m-1} e^{\mathrm{H}}(t-\tau_l)P_l e(t)+\sum_{l=1}^{m-1} e^{\mathrm{H}}(t)P_l e(t-\tau_l)\le\sum_{l=1}^{m-1} e^{\mathrm{H}}(t-\tau_l)e(t-\tau_l)+\sum_{l=1}^{m-1} e^{\mathrm{H}}(t)P_l^{\mathrm{H}}P_l e(t),$$

and

$$e^{\mathrm{H}}(t-\tau_l)P_0e(t)+e^{\mathrm{H}}(t)P_0e(t-\tau_l)\le e^{\mathrm{H}}(t)e(t)+e^{\mathrm{H}}(t)P_0^{\mathrm{H}}P_0e(t), \tag{14}$$

where $l=1,\ldots,m-1$.

Substituting inequality (14) into inequality (13), the following inequality is obtained:

$$\begin{aligned}
{}_{t_0}^{C}D_t^{\alpha}V(t) \le\ & r_2\sum_{l=1}^{m-1} e^{\mathrm{H}}(t-\tau_l)e(t-\tau_l)+r_2\sum_{l=1}^{m-1} e^{\mathrm{H}}(t)e(t)+\sum_{l=1}^{m-1} e^{\mathrm{H}}(t-\tau_l)e(t-\tau_l)\\
&+\sum_{l=1}^{m-1} e^{\mathrm{H}}(t)P_l^{\mathrm{H}}P_le(t)+e^{\mathrm{H}}(t)e(t)+e^{\mathrm{H}}(t)P_0^{\mathrm{H}}P_0e(t)-2\sum_{i=1}^{N} r_1e_i^{\mathrm{H}}(t)e_i(t)\\
&-2\lambda_i[\sum_{i=1}^{N}(e_i^{\mathrm{H}}(t)e_i(t))^{1-\rho}+\sum_{i=1}^{N}((\hat{\vartheta}(t)-\vartheta)^{\mathrm{H}}(\hat{\vartheta}(t)-\vartheta))^{1-\rho}+\sum_{i=1}^{N}((\hat{\beta}_i(t)-\beta_i)^{\mathrm{H}}(\hat{\beta}_i(t)-\beta_i))^{1-\rho}]\\
\le\ & e^{\mathrm{H}}(t)\left[r_2(m-1)+1+\sum_{l=1}^{m-1}\lambda_{\max}\left(P_l^{\mathrm{H}}P_l\right)-2r_1\right]e(t)+(r_2+1)\sum_{l=1}^{m-1} e^{\mathrm{H}}(t-\tau_l)e(t-\tau_l)\\
&-2\lambda_i\left[\sum_{i=1}^{N}(e_i^{\mathrm{H}}(t)e_i(t))^{1-\rho}+\sum_{i=1}^{N}((\hat{\vartheta}(t)-\vartheta)^{\mathrm{H}}(\hat{\vartheta}(t)-\vartheta))^{1-\rho}+\sum_{i=1}^{N}((\hat{\beta}_i(t)-\beta_i)^{\mathrm{H}}(\hat{\beta}_i(t)-\beta_i))^{1-\rho}\right].
\end{aligned} \tag{15}$$

Using Lemma 3, it follows that

$$\begin{aligned}
&\sum_{i=1}^{N}(e_i^{\mathrm{H}}(t)e_i(t))^{1-\rho}\ge\left[\sum_{i=1}^{N}(e_i^{\mathrm{H}}(t)e_i(t))\right]^{1-\rho},\\
&\sum_{i=1}^{N}((\hat{\vartheta}(t)-\vartheta)^{\mathrm{H}}(\hat{\vartheta}(t)-\vartheta))^{1-\rho}\\
\ge&\left[\sum_{i=1}^{N}(\hat{\vartheta}(t)-\vartheta)^{\mathrm{H}}(\hat{\vartheta}(t)-\vartheta)\right]^{1-\rho},\\
&\sum_{i=1}^{N}((\hat{\beta}_i(t)-\beta_i)^{\mathrm{H}}(\hat{\beta}_i(t)-\beta_i))^{1-\rho}\\
\ge&\left[\sum_{i=1}^{N}(\hat{\beta}_i(t)-\beta_i)^{\mathrm{H}}(\hat{\beta}_i(t)-\beta_i)\right]^{1-\rho}.
\end{aligned}$$

Therefore,

$$\begin{aligned}
&\sum_{i=1}^{N}(e_i^{\mathrm{H}}(t)e_i(t))^{1-\rho}+\sum_{i=1}^{N}((\hat{\vartheta}(t)-\vartheta)^{\mathrm{H}}(\hat{\vartheta}(t)-\vartheta))^{1-\rho}\\
&+\sum_{i=1}^{N}((\hat{\beta}_i(t)-\beta_i)^{\mathrm{H}}(\hat{\beta}_i(t)-\beta_i))^{1-\rho}\\
\ge&\left[\sum_{i=1}^{N}(e_i^{\mathrm{H}}(t)e_i(t))\right]^{1-\rho}+\left[\sum_{i=1}^{N}(\hat{\vartheta}(t)-\vartheta)^{\mathrm{H}}(\hat{\vartheta}(t)-\vartheta)\right]^{1-\rho}\\
&+\left[\sum_{i=1}^{N}(\hat{\beta}_i(t)-\beta_i)^{\mathrm{H}}(\hat{\beta}_i(t)-\beta_i)\right]^{1-\rho}\\
\ge&\left[\sum_{i=1}^{N}e_i^{\mathrm{H}}(t)e_i(t)+\sum_{i=1}^{N}\left(\hat{\vartheta}(t)-\vartheta\right)^{\mathrm{H}}\left(\hat{\vartheta}(t)-\vartheta\right)\right.\\
&\left.+\sum_{i=1}^{N}\left(\hat{\beta}_i(t)-\beta_i\right)^{\mathrm{H}}\left(\hat{\beta}_i(t)-\beta_i\right)\right]^{1-\rho}.
\end{aligned} \tag{16}$$

Considering Eq. (12) and substituting inequality (16) into inequality (15) at the same time, the following inequality is obtained:

$$\begin{aligned}
{}_{t_0}^{C}D_t^{\alpha}V(t)\le& e^{\mathrm{H}}(t)\left[r_2(m-1)+1+\sum_{l=1}^{m-1}\lambda_{\max}\left(P_l^{\mathrm{H}}P_l\right)-2r_1\right]e(t)\\
&+(r_2+1)\sum_{l=1}^{m-1} e^{\mathrm{H}}(t-\tau_l)e(t-\tau_l)-2\lambda V^{1-\rho}(t).
\end{aligned}$$

Then, it follows from inequalities (9) and (10) that

$${}_{t_0}^{C}D_t^{\alpha}V(t)\le-2\lambda V^{1-\rho}(t),$$

where λ is a positive constant, $1-\alpha<\rho<1$.

From Lemma 4, we obtain that networks (2) and (3) achieve synchronization, and the setting time t_1 is listed below.

$$t_1=t_0+\left(\frac{\Gamma(1+\alpha)\Gamma(\rho)V^{\alpha+\rho-1}(t_0)}{2\lambda\Gamma(\alpha+\rho)}\right)^{1/\alpha}$$

when $t_0=0$, $t_1=(\frac{\Gamma(1+\alpha)\Gamma(\rho)V^{\alpha+\rho-1}(0)}{2\lambda\Gamma(\alpha+\rho)})^{1/\alpha}$. Now, the proof ends here.

4. Numerical simulation and application to image encryption

4.1. Numerical examples

In this section, the Lorenz system and application to image encryption are used to verify the validity of the proposed theorem.

Example 1 Consider complex Lorenz system as the node dynamic system of network with five nodes as follows:

$$
{}_0^C D_t^{\alpha} x_i(t) = \begin{cases} a(x_{i2}-x_{i1}) \\ bx_{i1}-x_{i2}-x_{i1}x_{i3} \\ \dfrac{\bar{x}_{i1}x_{i2}+x_{i1}\bar{x}_{i2}}{2}-cx_{i3} \end{cases} = \underbrace{\begin{pmatrix} 0 \\ -x_{i2}-x_{i1}x_{i3} \\ \dfrac{\bar{x}_{i1}x_{i2}+x_{i1}\bar{x}_{i2}}{2} \end{pmatrix}}_{f(x_i(t))} + \underbrace{\begin{pmatrix} x_{i2}-x_{i1} & 0 & 0 \\ 0 & x_{i1} & 0 \\ 0 & 0 & -x_{i3} \end{pmatrix}}_{g(x_i(t))} \cdot \underbrace{\begin{pmatrix} a \\ b \\ c \end{pmatrix}}_{\Theta},
$$

where $\alpha = 0.95$, $\Theta = (a,b,c)^{\mathrm{T}} = (10,28,8/3)^{\mathrm{T}}$, $x_{i1}, x_{i2} \in C^n$, $x_{i3} \in R^n$, $i = 1,2,\ldots 5$. Chaotic behavior of fractional order complex Lorenz system is exhibited in Fig. 1.

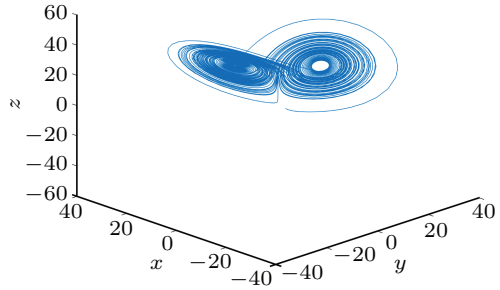


Fig. 1. Chaotic behavior of fractional order complex Lorenz system.

Consider the multi-link network with two different subnetworks, each with five nodes. The weight configuration matrixes A_0 and A_1 are respectively chosen as

$$
A_0 = \begin{bmatrix} -2 & 1 & 0 & 0 & 1 \\ 1 & -2 & 1 & 0 & 0 \\ 0 & 1 & -2 & 1 & 0 \\ 0 & 0 & 1 & -2 & 1 \\ 1 & 0 & 0 & 1 & -2 \end{bmatrix},
$$

$$
A_1 = \begin{bmatrix} -4 & 1 & 1 & 1 & 1 \\ 1 & -1 & 0 & 0 & 0 \\ 1 & 0 & -1 & 0 & 0 \\ 1 & 0 & 0 & -1 & 0 \\ 1 & 0 & 0 & 0 & -1 \end{bmatrix},
$$

where A_0 has no time-delay. Figure 2 shows the topological structures of two weighted subgraphs A_0 and A_1 respectively.

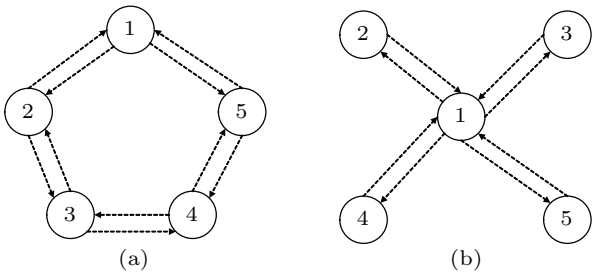


Fig. 2. Topological structures of two weighted subgraphs, showing (a) topological structures of weighted subgraph A_0 and (b) topological structure of weighted subgraph A_1.

The fractional-order complex-valued uncertain multi-links network containing five nodes is expressed as

$$
{}_0^C D_t^{\alpha} x_i(t) = f(x_i(t)) + g(x_i(t))\beta_i + \sum_{j=1}^{N} a_{ij}^0 \Gamma x_j(t) + \sum_{j=1}^{N} a_{ij}^1 \Gamma x_j(t-\tau_1) + u_i(t), \quad i = 1,2,\ldots,5. \tag{17}
$$

And the synchronous node is

$$
{}_0^C D_t^{\alpha} s(t) = f(s(t)) + g(s(t))\vartheta. \tag{18}
$$

The controller is designed as

$$
\begin{aligned} u_i(t) = & -f(x_i(t)) - g(x_i(t))\hat{\beta}_i(t) \\ & + v\left(f(s(t)) + g(s(t))\hat{\vartheta}(t)\right) \\ & - r_1 e_i(t) - \frac{\lambda e_i(t)}{[e_i^{\mathrm{H}}(t)e_i(t)]^{\rho}} + r_2 e_i(t-\tau_1), \end{aligned} \tag{19}
$$

where $\hat{\vartheta}(t) = \left(\hat{\vartheta}_1(t), 28, 8/3\right)^{\mathrm{T}}$, $\hat{\beta}_i(t) = \left(10, \hat{\beta}_{i2}(t), 8/3\right)^{\mathrm{T}}$, $\hat{\vartheta}_1(t)$, $\hat{\beta}_{i2}(t)$ are determined by parameter update laws as follows:

$$
\begin{aligned} {}_0^C D_t^{\alpha} \hat{\vartheta}_1(t) = & -(s_2(t) - s_1(t))^{\mathrm{H}} v^{\mathrm{H}} e_{i1}(t) \\ & - \frac{\lambda(\hat{\vartheta}_1(t) - \vartheta_1)}{[(\hat{\vartheta}(t) - \vartheta)^{\mathrm{H}}(\hat{\vartheta}(t) - \vartheta)]^{\rho}}, \end{aligned} \tag{20}
$$

$$
{}_0^C D_t^{\alpha} \hat{\beta}_{i2}(t) = x_{i1}^{\mathrm{H}}(t) e_{i2}(t) - \frac{\lambda(\hat{\beta}_{i2}(t) - \beta_{i2})}{[(\hat{\beta}_i(t) - \beta_i)^{\mathrm{H}}(\hat{\beta}_i(t) - \beta_i)]^{\rho}}. \tag{21}
$$

Select the inner coupling matrix as

$$
\Gamma = \begin{bmatrix} 1 & 0 & 0 \\ 0 & 1 & 0 \\ 0 & 0 & 1 \end{bmatrix},
$$

$r_1 = 15$, $r_2 = -5$, $\tau_1 = 0.3$, $\lambda = 5$, $\rho = 0.2$, $v = 2+3\mathrm{j}$. The initial values are given as follows: $s(0) = (1+0.2\mathrm{j}, 2+0.3\mathrm{j}, 3)^{\mathrm{T}}$, $x_i(0) = (2+0.2i+0.5\mathrm{j}, 3+0.2i+0.6\mathrm{j}, 4+0.2i)^{\mathrm{T}}$, $\hat{\vartheta}_1(0) = 12$, and $\hat{\beta}_{i2}(0) = 25$, where $i = 1,2,\ldots,5$.

According to Theorem 1, $\lambda_{\max}\left(P_l^{\mathrm{H}} P_l\right) = 25$, $m = 2$, $r_2(m-1) + 1 + \sum_{l=1}^{m-1} \lambda_{\max}\left(P_l^{\mathrm{H}} P_l\right) - 2r_1 = -9 < 0$, and $r_2 + 1 = -4 < 0$ satisfy inequalities (9) and (10), then network (17) can

achieve CPS with Eq. (18) within the limited time, and we obtain the estimation t_1

$$\begin{aligned} t_1 &= t_0 + \left(\frac{\Gamma(1+\alpha)\Gamma(\rho)V^{\alpha+\rho-1}(t_0)}{2\lambda\Gamma(\alpha+\rho)}\right)^{1/\alpha} \\ &= 0 + \left(\frac{\Gamma(1+0.95)\Gamma(0.2)\times 711.5000^{0.95+0.2-1}}{2\times 5\times\Gamma(0.95+0.2)}\right)^{1/0.95} \\ &= 1.3087. \end{aligned}$$

Figure 3 shows the trajectories of synchronization error $e_i(t)$ $(i=1,2,\ldots,5)$ We can see that $e_i(t)=0$ $(i=1,2,\ldots,5)$ when $t \geq 1.3087$, which denotes that the networks (17) and (18) can accomplish CPS in a finite time. Figure 4 displays the trajectories of uncertain parameters. Moreover, we observe from Fig. 4 that $\vartheta_1 \to 10$ and $\beta_{i2} \to 28$ within a finite time interval, which indicates that the uncertain parameters are successfully identified.

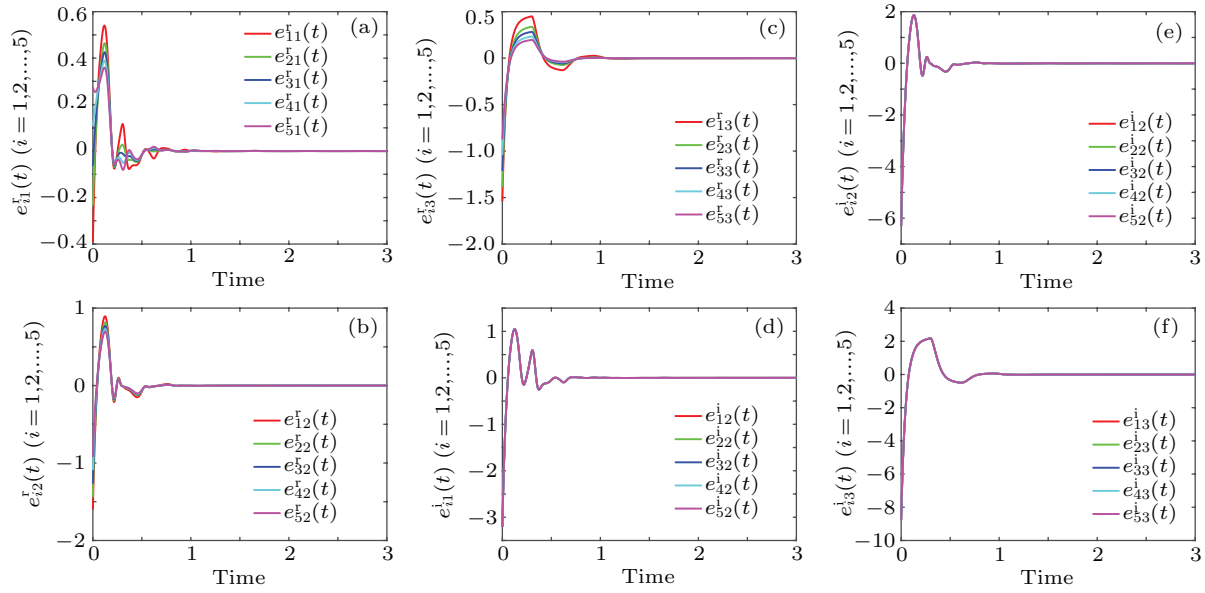


Fig. 3. Synchronization errors $e_i(t)$ $(i=1,2,\ldots,5)$ of networks (17) and (18), showing [(a), (c), and (e)] real part of synchronization error, and [(b), (d), and (f)] imaginary part of synchronization error.

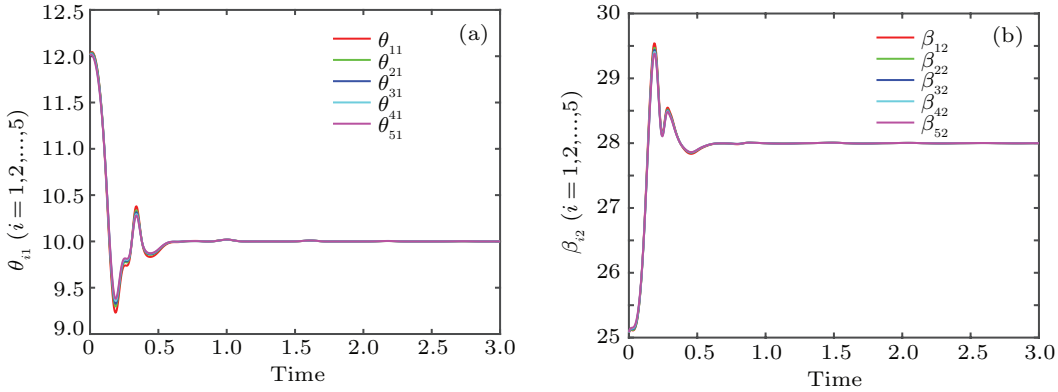


Fig. 4. Uncertain parameters of the networks (17) and (18): (a) estimation of ϑ_1 (b) estimation of β_{i2}.

In the following Figs. 5–10, we display the relations between the estimated t_1 and the fractional-order parameter α and the control parameters ρ and λ. From Fig. 5, we can observe that the estimated t_1 increases with the growth of the the fractional-order α. From Fig. 6, we can observe that the estimated t_1 firstly decreases as the control parameter ρ increases, then it increases as the ρ increases. From Fig. 7, we can see that the estimated t_1 decreases with the control parameter λ increasing.

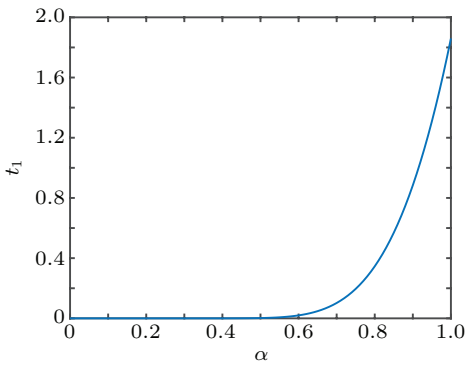


Fig. 5. Relations between estimated t_1 and α.

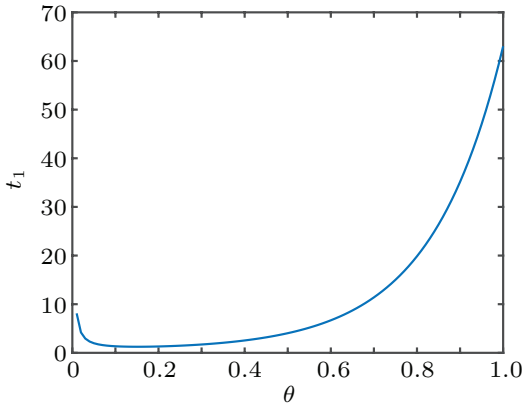


Fig. 6. Relations between estimated t_1 and ρ.

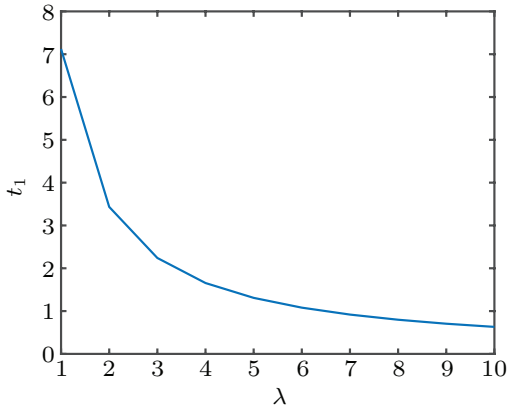


Fig. 7. Relation between estimated t_1 and λ.

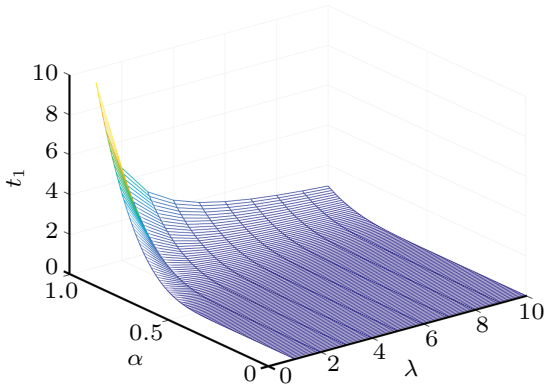


Fig. 8. Relations between estimated t_1 and α, λ.

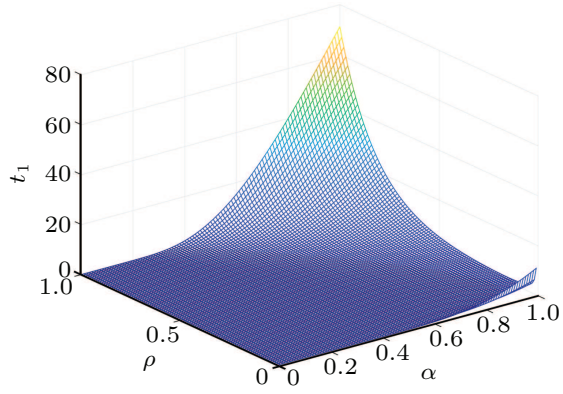


Fig. 9. Relations between estimated t_1 and ρ, α.

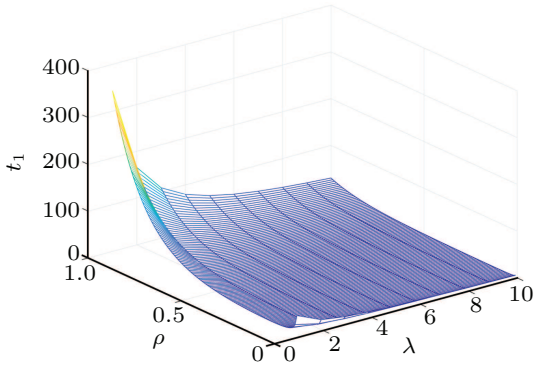


Fig. 10. Relations between estimated t_1 and ρ, λ.

Example 2 Based on synchronization results derived in Example 1, we apply them to image encryption. We take the network (17) as the encryption chaotic sequences to realize the image encryption and the synchronous node (18) as the decryption chaotic sequences to realize image decryption.

Here, we use the image encryption scheme on DNA coding. The DNA sequence consists of A (adenine), G (guanine), C (cytosine), and T (thymine), where A and T, G and C are two complementary base pairs. Owing to 0 and 1 being complementary in binary, we can encode four nucleic acids A, C, G and T with 00, 01, 10, and 11. Table 1 gives 8 kinds of encoding combinations which satisfy the Watson-Crick complement rule. Table 2 show the addition, subtraction and XOR operations of DNA sequences.

Table 1. Rules of DNA coding.

	1	2	3	4	5	6	7	8
00	A	A	G	G	C	C	T	T
01	C	G	A	T	A	T	G	C
10	G	C	T	A	T	A	C	G
11	T	T	C	C	G	G	A	A

Table 2. Operations of DNA sequences.

	+				−				$\oplus$			
	A	C	G	T	A	C	G	T	A	C	G	T
A	A	C	G	T	G	C	C	G	C	G	A	T
C	C	G	T	A	A	T	A	A	G	C	T	A
G	G	T	A	C	T	A	T	T	A	T	C	G
T	T	A	C	G	C	G	G	C	T	A	G	C

4.2. Processes of image encryption and decryption

We use the fractional order complex-valued uncertain multi-links network to generate chaotic sequences to disturb the pixels of original image. The encryption flowchart is shown in Fig. 11, which includes the generation of chaotic sequence and encryption of image by DNA coding and chaotic sequence.

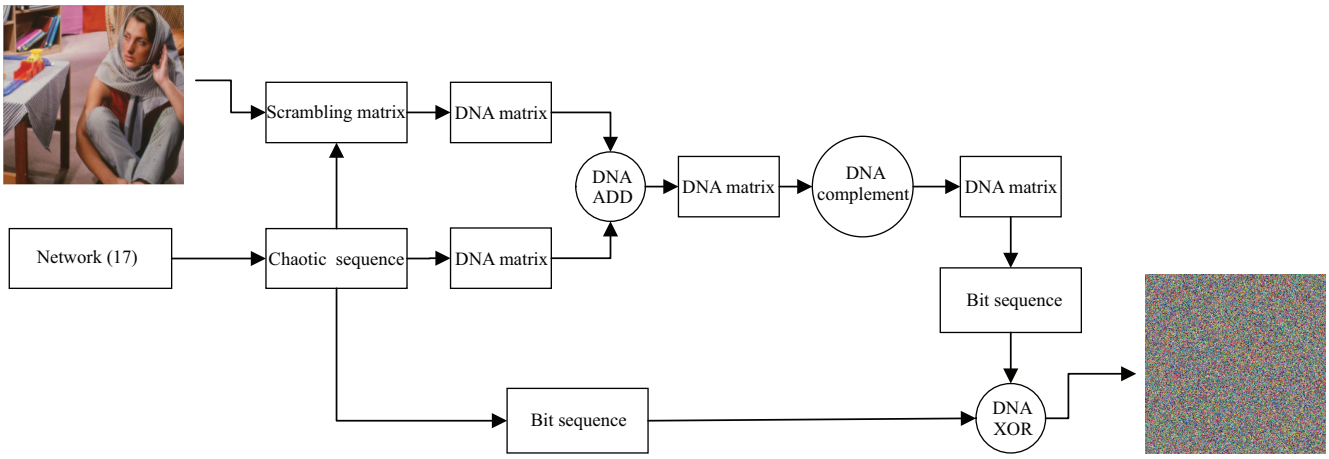


Fig. 11. Flowchart of encryption.

4.2.1. Generate chaotic sequence

Step 1 The fractional order complex-valued uncertain multi-links network is iterated N_0+mn times, and the last mn iterations are regarded as valid data, then the four state values $x_i(1), x_i(2), x_i(3)$, and $x_i(1)+x_i(2)$, $i=1,2,3,\ldots,mn$ are obtained.

Step 2 Four state values are used to generate sequences $s(i,j)\in[0,255]$, $s'(i,j)\in[0,255]$, $j=1,2,3,4$. The calculation formulas are as follows:

$$\begin{aligned} s(i,j) &= \mathrm{mod}\{\mathrm{floor}((|x_i(j)|-\mathrm{floor}(|x_i(j)|))\times 10^7),256\}, \quad j=1,2,3,4,\\ s'(i,j) &= \mathrm{mod}\left\{\mathrm{floor}\left(\mathrm{mod}\left(\left((|x_i(j)|-\mathrm{floor}(|x_i(j)|))\times 10^{15}\right),10^8\right)\right),256\right\}, \quad j=1,2,3,4, \end{aligned} \tag{22}$$

where mod( ) denotes the modulo operation and floor( ) refers to the flooring operation.

$$s(i)=\left[s(i,1),s(i,2),s(i,3),s(i,4),s'(i,1),s'(i,2),s'(i,3),s'(i,4)\right]. \tag{23}$$

Step 3 A chaotic sequence k is generated as follows:

$$k=[s(1),s(2),\ldots,s(mn)]. \tag{24}$$

4.2.2. Image encryption process

Step 1 Select $m\times n\times 3$ color image I as the encrypted image which is composed of R, G, and B channels.

Scrambling the pixel values of R, G, and B channels in the color image I into I^{R}, I^{G}, I^{B} through chaotic sequence k and using DNA encryption rules for I^{R}, I^{G}, I^{B}, we obtain the DNA sequences D_i^{R}, $\{D_i^{\mathrm{G}}\}$, $\{D_i^{\mathrm{B}}\}$, $i=1,2,\ldots,4mn$.

Step 2 Choose addition operation of DNA sequences, then we will encode sequences D_i^{R}, $\{D_i^{\mathrm{G}}\}$, $\{D_i^{\mathrm{B}}\}$, $i=1,2,\ldots,4mn$ to obtain new sequences D_{1i}^{R}, $\{D_{1i}^{\mathrm{G}}\}$, $\{D_{1i}^{\mathrm{B}}\}$, $i=1,2,\ldots,4mn$ as follows:

$$\begin{cases} D_{11}^j = d_0 + D_1^j, \\ D_{1i}^j = D_{i-1}^j + D_i^j, \end{cases} \tag{25}$$

with $i=2,3,\ldots,4mn$, $j\in\{\mathrm{R},\mathrm{G},\mathrm{B}\}$, where $d_0\in\{A,C,G,T\}$ is the initial nucleic acid.

Step 3 Using other DNA encryption rules for sequence k, we obtain the sequence k_1. Then, we perform DNA addition operation for k_1 and D_{1i}^{R}, $\{D_{1i}^{\mathrm{G}}\}$, $\{D_{1i}^{\mathrm{B}}\}$, $i=1,2,\ldots,4mn$ to obtain D_{2i}^{R}, $\{D_{2i}^{\mathrm{G}}\}$, $\{D_{2i}^{\mathrm{B}}\}$, $i=1,2,\ldots,4mn$.

Step 4 According to the binary k_2 sequence, we take the complement of D_{2i}^{R}, $\{D_{2i}^{\mathrm{G}}\}$, $\{D_{2i}^{\mathrm{B}}\}$, $i=1,2,\ldots,4mn$ to obtain D_{3i}^{R}, $\{D_{3i}^{\mathrm{G}}\}$, $\{D_{3i}^{\mathrm{B}}\}$, $i=1,2,\ldots,4mn$.

Step 5 Using any of the DNA encryption rules to decode DNA sequences D_{3i}^{R}, $\{D_{3i}^{\mathrm{G}}\}$, $\{D_{3i}^{\mathrm{B}}\}$, $i=1,2,\ldots,4mn$, then sequences I_1^{R}, I_1^{G}, I_1^{B} can be obtained.

Step 6 Performing bit XOR operation for sequences k and I_1^{R}, I_1^{G}, I_1^{B} to gain I_2^{R}, I_2^{G}, I_2^{B}, then let I_2^{R}, I_2^{G}, I_2^{B} convert into the cipher image Q^{R}, Q^{G} and Q^{B}.

The decryption process can be gained by inverting the encryption process.

4.3. Simulation results and security analyses

We select the color image with the size of $256\times256\times3$ as the original image, which is depicted in Fig. 12(a). Using the encryption algorithm, we obtain the encrypted image in Fig. 12(b). It has no trace of the original image. The decrypted-image is shown in Fig. 12(c).

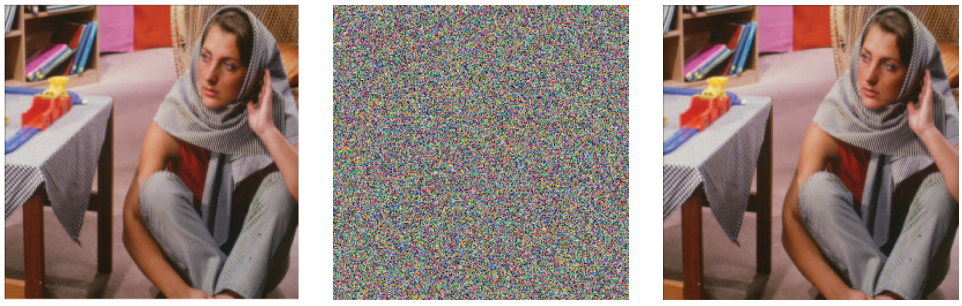


Fig. 12. Image encryption and decryption results, showing (a) original image, (b) encrypted image, and (c) decrypted image.

As for encrypted image, it must be secure and can resist different security attacks. For this, we analyze the security from the histogram distributions and correlation coefficients.

4.3.1. Histograms test

The distribution of image pixel intensity values can be evaluated by histogram. We can see that the histograms of the encrypted image are equally distributed which can protect the original image information and resist the statistical attack. Figures 13(a)–13(f) display the histograms of the original image and encrypted image in the R, G, and B channels, respectively.

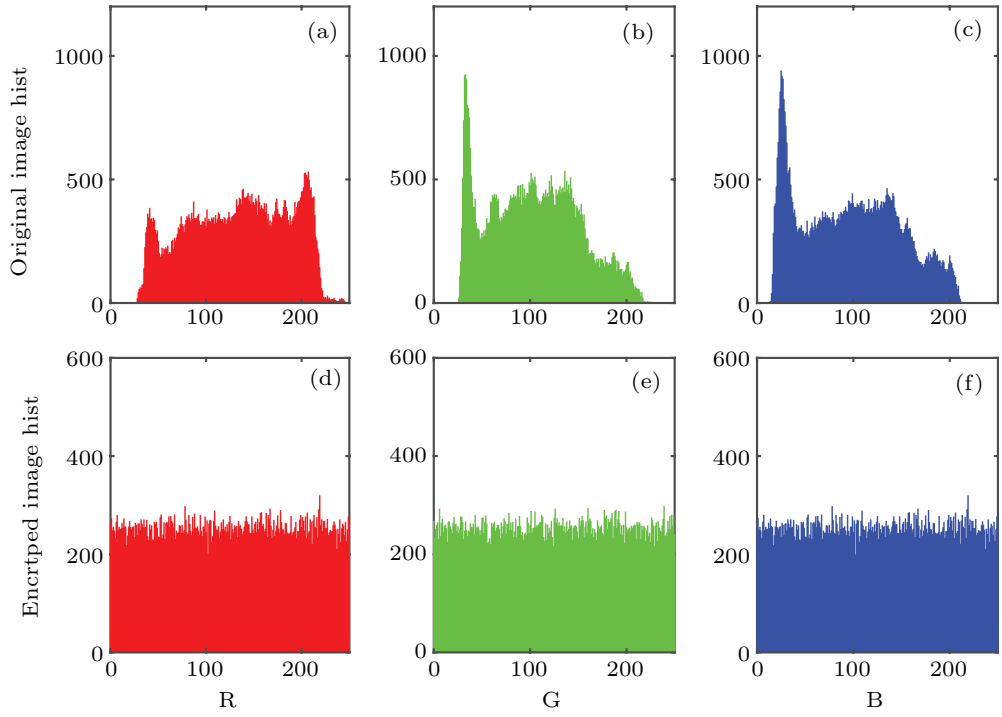


Fig. 13. Histograms of [(a)–(c)] original images and [(d)–(f)] encrypted images.

4.3.2. Correlation coefficient analysis

The correlation of adjacent pixels reflects the correlation degree of pixel values at the adjacent positions of images.

Generally, we calculate the correlations of adjacent pixels in horizontal, vertical, and diagonal directions from the following formula:

$$r_{xy} = \frac{\operatorname{cov}(x,y)}{\sqrt{D(x)\,D(y)}}, \tag{26}$$

where x and y are the pixel values of two adjacent pixels, N denotes$N$ pairs of adjacent pixels selected, and

$$\operatorname{cov}(x,y) = \frac{1}{N}\sum_{i=1}^{N}[x_i - E(x)]\,[y_i - E(y)], \quad E(x) = \frac{1}{N}\sum_{i=1}^{N} x_i,$$

$$D(x) = \frac{1}{N}\sum_{i=1}^{N}[x_i - E(x)]^2.$$

From Fig. 14 and Table 3, we can observe that correlations of adjacent pixels in the original image are high, but in the encrypted image, the correlations are efficiently reduced, which indicates that the encrypted image can effectively hide the information about original image.

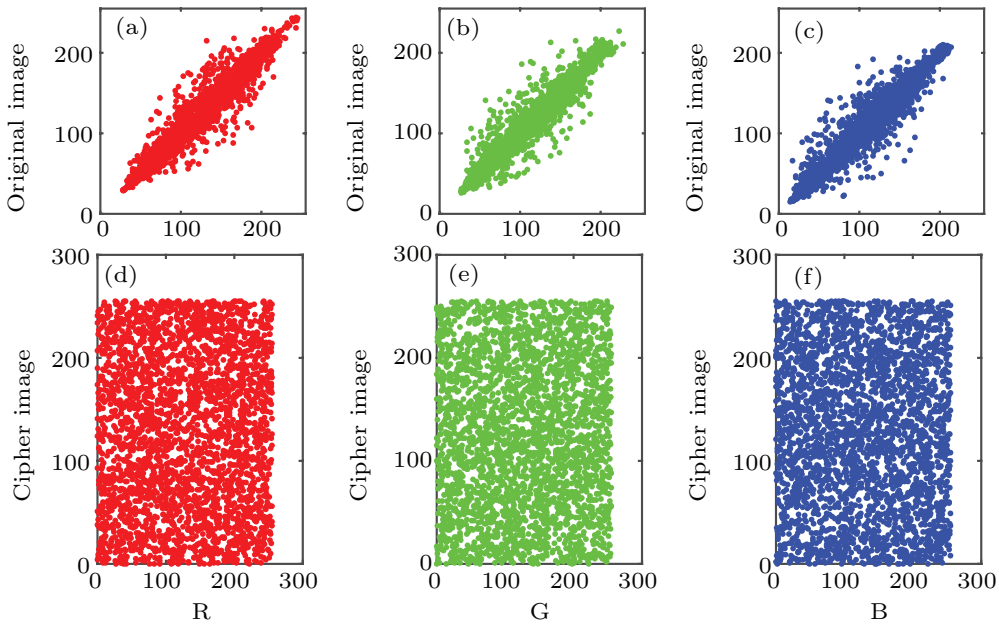


Fig. 14. Correlation of adjacent pixels in horizontal directions, showing [(a)–(c)] original images and [(d)–(f)] encrypted images.

Table 3. Correlation coefficients of adjacent pixels in original images and encrypted images.

	Original image			Encrypted image		
	R	G	B	R	G	B
Horizontal	0.9514	0.9473	0.9530	3.4429×10^{-4}	0.0033	–0.0022
Vertical	0.9695	0.9679	0.9714	7.5907×10^{-4}	0.0017	0.0044
Diagonal	0.9415	0.9367	0.9436	–0.0011	8.5756×10^{-4}	–0.0027

5. Conclusions

This paper addresses FTCPS problem of fractional order complex-valued uncertain multi-link networks. Considering the uncertain parameters, the adaptive controller and parameter update laws are designed. On the basis of fractional-order Lyapunov functional method and finite-time stability theory, the criteria of FTCPS in fractional-order complex-valued multi-link network are derived. In addition, the relationship between synchronization time and fractional order and control parameters are analyzed. Finally, simulation example and image encryption application are provided to verify the correctness of the obtained results. In the future, we will study the finite-time function projective synchronization in fractional order complex multi-links networks with time-varying delay.

References

[1] Zhao H, Li L X, Xiao J H, Yang Y X and Zheng M W 2017 *Chaos, Solitons and Fractals* **104** 268

[2] Zhao H, Li L X, Peng H P, Xiao J H and Yang Y X 2015 *Eur. Phys. J. B* **88** 45

[3] Zhao H, Li L X, Peng H P, Xiao J H, Yang Y X and Zheng M W 2016 *Nonlinear Dyn.* **83** 1437

[4] Hu Q Y, Peng H P, Wang Y G, Hu Z R and Yang Y X 2012 *Nonlinear Dyn.* **69** 1813

[5] Xu Y, Wang Q, Li W X and Feng J Q 2021 *Mathematical Methods in the Applied Sciences* **44** 3356

[6] Peng H P, Wei N, Li L X, Xie W S and Yang Y X 2010 *Phys. Lett. A* **374** 2335

[7] Li L X, Kurths J, Peng H P, Yang Y X and Luo Q 2013 *Eur. Phys. J. B* **86** 125

[8] Wang X and Miao P 2020 *Int. J. Control Autom. Syst.* **18** 1993

[9] Li L X, Li W W, Kurths J, Luo Q, Yang Y X and Li S D 2015 *Chaos, Solitons and Fractals* **72** 20

[10] Li K Z, He E, Zeng Z R and Tse C K 2013 *Chin. Phys. B* **22** 070504

[11] Wang S G and Yao H X 2012 *Chin. Phys. B* **21** 050508

[12] Aadhithiyan S, Raja R, Zhu Q X and Alzabut J 2021 *Neural Process. Lett.* **53** 1035

[13] Wang J Y, Zhang H G, Wang Z S and Liang H J 2013 *Chin. Phys. B* **22** 090504

[14] Sha H S, Wang G J, Hao T and Wang Z X 2020 *Complexity* **2020** 3742876

[15] Ding D W, Yao X L and Zhang H W 2020 *Neural Process. Lett.* **51** 325

[16] Yang X S and Cao J D 2010 *Appl. Math. Model.* **34** 3631

[17] Li J R, Jiang H J, Hu C and Yu J 2018 *Chaos, Solitons and Fractals* **114** 291

[18] Wang W P, Peng H P, Li L X, Xiao J H and Yang Y X 2015 *Neural Process. Lett.* **41** 71

[19] Zhao H, Li L X, Peng H P, Xiao J H, Yang Y X and Zheng M W 2017 *Modern Phys. Lett. B* **31** 1750008

[20] Zheng M W, Li L X, Peng H P, Xiao J H, Yang Y X, Zhang Y P and Zhao H 2019 *Commun. Nonlinear Sci. Numer. Simulat.* **67** 108

[21] Li H L, Cao J D, Hu C, Zhang L and Wang Z L 2019 *Neurocomputing* **356** 31

[22] Bao H B, Park J H and Cao J D 2021 *IEEE Transactions on Neural Networks and Learning Systems* **32** 3230

[23] Ding D W, Yan J, Wang N and Liang D 2017 *Commun. Theor. Phys.* **68** 366
[24] Ding D W, Yan J, Wang N and Liang D 2017 *Chaos, Solitons and Fractals* **104** 41
[25] Yang S, Yu J, Hu C and Jiang H J 2018 *Neural Networks* **104** 104
[26] Xu Y, Li Y Z and Li W X 2020 *Commun. Nonlinear Sci. Numer. Simulat.* **85** 105239
[27] Yang X S and Cao J D 2014 *Appl. Math. Comput.* **227** 480
[28] Banu L J and Balasubramaniam P 2016 *Neurocomputing* **179** 126
[29] Zhang C, Wang X Y, Luo C, Li J Q and Wang C P 2018 *Physica A* **494** 251
[30] Wu Z Y, Liu D F and Ye Q L 2015 *Commun. Nonlinear Sci. Numer. Simulat.* **20** 273
[31] Li H L, Cao J D, Jiang H J and Alsaedi A 2019 *Physica A* **533** 122027
[32] Du L, Yang Y and Lei Y M 2018 *Appl. Math. Mech.-Engl. Ed.* **39** 353
[33] Yang X Y, Li X D and Duan P Y 2022 *Neural Comput. Appl.* **34** 5097
[34] Zhang L M, Sun K H, Liu W H and He S B 2017 *Chin. Phys. B* **26** 100504
[35] Wang Y Z and Yang F F 2021 *Phys. Scr.* **96** 035209
[36] Kumar M, lqbal A and Kumar P 2016 *Signal Process.* **125** 187
[37] Chai X L, Gan Z H, Yuan K, Chen Y R and Liu X X 2019 *Neural Comput. Appl.* **31** 219
[38] Xu Y and Li W X 2020 *Physica A* **549** 123903
[39] Wu Z Y and Fu X C 2013 *Nonlinear Dyn.* **72** 9
[40] Xu Q, Zhuang S X, Liu S J and Xiao J 2016 *Neurocomputing* **186** 119
[41] Ding D W, Yao X L and Wang N 2019 *Int. J. Theor. Phys.* **58** 2357
[42] Ji G J, Hu C, Yu J and Jiang H J 2018 *J. Frankl. Inst.* **355** 4665
[43] Li H L, Cao J D, Jiang H J and Alsaedi A 2018 *J. Frankl. Inst.* **355** 5771